Diamond & Related Materials 20 (2011) 917–921

Contents lists available at ScienceDirect

Diamond & Related Materials

journal homepage: www.elsevier.com/locate/diamond

Electron emission from CVD diamond *p–i–n* junctions with negative electron affinity during room temperature operation☆☆

D. Takeuchi [a,*], T. Makino [a], H. Kato [a], M. Ogura [a], N. Tokuda [b], K. Oyama [a,c], T. Matsumoto [a,c], H. Okushi [a], S. Yamasaki [a,c]

[a] Energy Technology Research Institute, National Institute of Advanced Industrial Science and Technology (AIST), 1-1-1 Umezono, Tsukuba 305–8568, Japan
[b] Institute of Science and Engineering, Kanazawa University, Kakuma-machi, Kanazawa 920–1192, Japan
[c] Graduate School of Pure and Applied Science, University of Tsukuba, Tsukuba 305–8577, Japan

ARTICLE INFO

Available online 14 May 2011

Keywords:
Diamond
p–n junction diode
Exciton
Electron emission
Negative electron affinity

ABSTRACT

We successfully observed electron emission from hydrogenated diamond *p–i–n* junction diodes with negative electron affinity during room temperature operation. The emissions started when the applied bias voltage produced flat-band conditions, where the capacitance–voltage characteristics showed carrier injection in the *i*-layer. In this low current injection region, the electron emission efficiency (η) of the *p–i–n* junction diodes (*p* is top layer) was about 5×10^{-5}, while that of the *n–i–p* diodes (*n* is top layer) was about 10^{-8}. With increasing diode current, both diodes showed an increase in η and a nonlinear increase in emission current. In the high current injection region with high diode current of 5–50 mA, both diodes had an emission current of almost 10 μA, where η of a *p–i–n* junction diode was 0.18%, while that of a *n–i–p* junction diode was 0.02%.
Note that η, which corresponds to the electron emission mechanism, depended on the diode current level.

1. Introduction

Because of its low or negative electron affinity (NEA), [1–3] diamond is expected to form a superior cold cathode with high efficiency and high net current (or high current density).

Many studies have reported high electron emission efficiencies with newly developed unique structures of diamond electron emission devices [2,4–7]. For practical use of NEA, further investigations are required to perform high net current (or high current density) operations with practical use of NEA.

Recently, Koizumi et al. successfully demonstrated electron emission from {111} *p–n* junction diodes with a hydrogen (H-) terminated surface [8,9]. Although there was scope for further development of the device structure, a high electron emission efficiency of $\eta>1\%$ and an emission current of 1 μA were achieved. This structure appears to be one of the solutions for realizing the practical use of NEA using diamond [10,11]. The device performance was mainly reported at higher temperatures of 200–300 °C to activate deep donor levels of phosphorous atoms in the *n*-type diamond [12,13]. However, high electron emission current during room temperature (RT) operation is an essential requirement for electronic devices using the unique NEA properties.

Based on photoelectron emission experiments for diamond NEA surfaces, we concluded that free excitons clearly played an important role in the electron emission mechanism from these emitters based on the *p–n* junction diodes [1,3,14]. Thus, when the number of free excitons (or the density of free excitons) increases during RT operation, higher electron emission currents (or higher electron emission efficiency) can be expected [1,3,14,15].

Makino et al. have successfully demonstrated strong deep-ultraviolet (DUV) luminescence ($h\nu=235$ nm) due to free exciton recombination from a diamond light-emitting-device (DUV-LED), which attained 0.3 mW during RT operation [16,17].

Based on the DUV-LED experimental results, we observed that the *p–i–n* junction structure (as opposite to a *p–n* junction structure) allows high current injection during RT operation because the intrinsic (*i*-) layer introduces better junction quality. In addition, the *i*-layer increases the life time of free excitons that results in a higher degree of DUV luminescence, which can be attributed to the higher-density of free excitons [17].

Based on the advanced techniques used by the diamond DUV-LEDs to obtain a high number (or high density) of free excitons, we aimed at realizing high current diamond-based *p–i–n* junction emitters with NEA during RT operation. We fabricated two types of *p–i–n* junction diodes: (a) *p–i–n*$^+$ diode with *p* top layer, and (b) *n–i–p–p*$^+$ diode with *n* top layer, using almost the same series resistances that are mainly attributed

☆☆ Presented at the Diamond 2010, 21st European Conference on Diamond, Diamond- Like Materials, Carbon Nanotubes, and Nitrides, Budapest.

* Corresponding author. Tel.: +81 29 861 5634; fax: +81 29 861 2773.
E-mail address: d.takeuchi@aist.go.jp (D. Takeuchi).

0925-9635/$ – see front matter © 2011 Elsevier B.V. All rights reserved.
doi:10.1016/j.diamond.2011.05.009

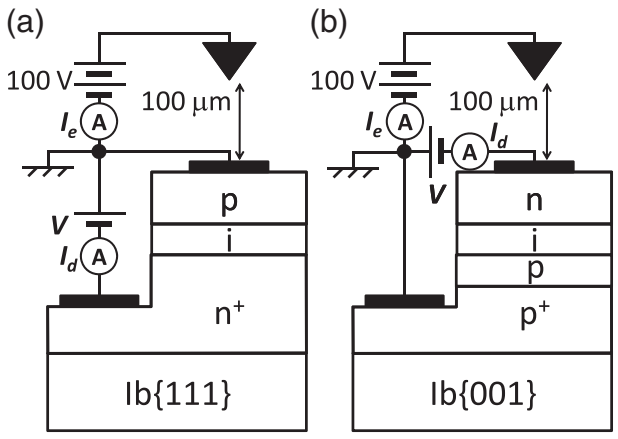

Fig. 1. Schematic diagrams of diode structures and electric circuits to operate each diode; (a) p–i–n^+ diode with p top layer, (b) n–i–p–p^+ diode with n top layer.

to the n-type layers. Here, there is a collector electrode above the "top-layers," as shown in Fig. 1. Based on the results obtained, we discuss the electron emission mechanism of the diamond p–i–n junction diodes having NEA.

2. Experiment

In order to fabricate diamond p–i–n junction diodes, each layer was grown by microwave-assisted plasma chemical vapor deposition (CVD). The substrate was a high-pressure and -temperature synthesized Ib-type {111} diamond with a 2.34° misorientation angle for the p–i–n^+ diode, and Ib-type {001} diamond with a 0.19° misorientation angle for the n–i–p–p^+ diode. Note that the order of p,i,n is denoted from the top- to the bottom-layers of the diodes as shown in Fig. 1. The n^+-layer implies that the phosphorous impurity concentration in the layer is around 10^{20} cm^{-3}, and this layer exhibits hopping conduction with a resistivity of about 100 Ω cm [18]. The p^+-layer implies that the boron impurity concentration in the layer is also around 10^{20} cm^{-3}, and this layer exhibits hopping conduction with a resistivity of about 3×10^{-2} Ωcm [19–23]. The other p, i and n represent layers with band conduction.

For characterization, both diode current–voltage (I_d–V) and emission current–voltage (I_e–V) characteristics were measured in an ultra high vacuum ($<10^{-7}$ Pa) at RT. Schematic diagrams for the electric circuits are also shown in Fig. 1. For electron emission measurements, the collector electrode voltage was fixed at 100 V with a distance of 100 μm between the collector electrode and the samples. The C–V characteristics were also measured using an LCR meter with small signals of 0.05 V and 1 kHz at RT [17,24]. The I–V characteristics were measured both before and after hydrogenation by hydrogen radical irradiation with a hot filament system [3]. Before the measurement after hydrogenation, the samples were annealed at 600 °C for 30 min to avoid the surface conductivity of H-termianted diamond surfaces due to the presence of surface adsorbates [25,26].

3. Results

3.1. n–i–p–p^+ junction diode

The growth condition for each layer of the n–i–p–p^+ diode is shown in Table 1. The thickness and doping profiles of each n-, i-, p-, and p^+-layer were measured using secondary ion mass spectroscopy (SIMS). The mesa structure was prepared using the photolithography and dry etching processes. Finally, Ti/Pt/Au electrodes were deposited on both the n- and p^+-layers. The growth condition for each layer was the same as that used in our previous works [13,19,27].

Table 1
Growth conditions for fabrication of n–i–p–p^+ junction diodes. TMB is trimethylboron.

Substrate off-angle: 0.19°	n-layer	i-layer	p-layer	p^+-layer
Source gas	$PH_3/CH_4/H_2$	CH_4/H_2	$B_2H_6/CH_4/H_2$	$TMB/CH_4/H_2$
Substrate temperature [°C]	900	800	800	800
C/H_2 ratio [%]	0.4	0.025	0.3	0.6
(Impurity gas)/CH_4 ratio	P/C 5%	–	B/C 50 ppm	B/C 1000 ppm
Gas pressure [Torr]	25	25	25	50
Microwave power [W]	750	750	750	1200
Thickness designed [μm]	0.7	0.1	1	>10

Fig. 2 shows a SIMS result for this sample. Although the interface roughness at each n–i or i–p junction resulted in the deterioration of the spatial resolution of depth profiles for both the phosphorous and boron atoms near these junctions, i-layer was observed between the phosphorous and boron layers at a depth of approximately 800 nm. The thickness of the i-layer was estimated to be less than or equal to 100 nm, where the phosphorous and boron profiles began to drop. As shown in Fig. 2, the n–i–p–p^+ junction was obtained as according to the design.

The concentration of boron impurity atoms in the p^+-layer was almost 10^{20} cm^{-3}. The other n- and p-layers were 700 and 1200 nm thick, respectively. The n-layer became the main component of the series resistance. The concentration of phosphorous atoms in the p-layer and that of boron atoms in the n-layer were below the detection limit of the SIMS measurements as shown in Fig. 2.

Fig. 3 shows the results of the C–V and $1/C^2$–V characteristics at 1 kHz for a n–i–p–p^+ junction diode at RT. Quality factors of the C–V measurement ranged from 10 to 4 for the range of −20 to 5 V. As $Q<10$, the accuracy of the C values should be determined carefully. However, the dependence of C on V was clear enough for us to consider the behavior of the depletion region and free carriers in this diode. In addition, the C value at −20 V was almost the same as the value calculated from the permittivity, diode area, and the width of the evaluated depletion layer using the space charge density value obtained by SIMS measurement.

As shown in the figure, the capacitance increased gradually as the bias voltage increased from −20 to +4 V (region I denoted in Fig. 3). This trend indicated the existence of a space-charge layer that extended to the p- and n-layers and narrowed as the bias voltage changed from −20 to +4 V. At around 4 to 8 V, once the slope of the C–V curve decreased (region II), the capacitance increased drastically as the bias voltage increased (region III). The constant capacitance at around 4–8 V may correspond to that of the intrinsic layer. The drastic increase of the capacitance for bias voltages higher than 8 V may correspond to changes due to carrier injection in the intrinsic layer. The effective built-in potential of 8 V was higher than what was

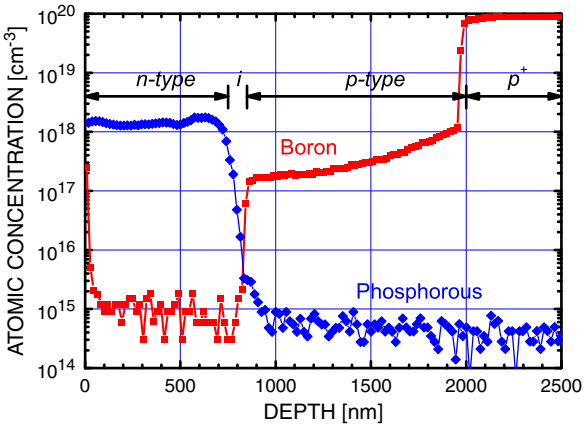

Fig. 2. Secondary ion mass spectroscopy (SIMS) results for the n–i–p–p^+ junction diodes.

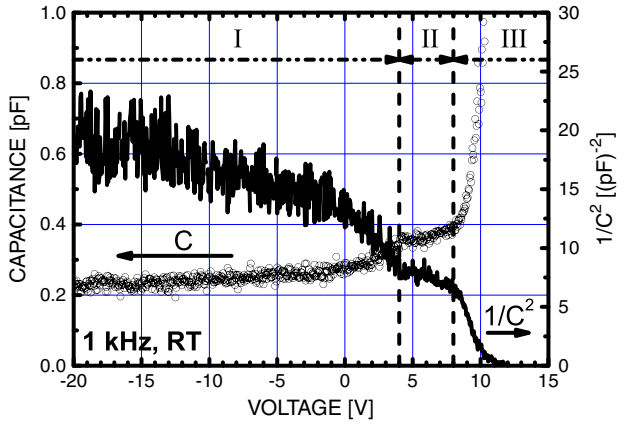

Fig. 3. C–V and $1/C^2$–V characteristics at 1 kHz of a n–i–p–p^+ junction diode at RT. The capacitance increased gradually as the bias voltage increased from −20 to +4 V (region I). At around 4–8 V, once the slope of the C–V curve became small (region II), the capacitance increased drastically as the bias voltage increased (region III).

expected for the diamond p–i–n diode (4.6 V). The effective built-in potential appeared to exhibit an additional voltage drop at the contact for the n-layer. These results were very similar to those obtained in previous publications [17,28]. Further investigations are currently in progress to more accurately evaluate the quantitative properties of the diode.

Fig. 4 shows the dependence of the diode (I_d: filled squares) and emission currents (I_e: filled circles) on the applied voltage. The electron emission efficiency ($\eta = I_e/I_d$) is represented by a solid line. The electrode for the p-type layer was grounded as shown in Fig. 1 (b), and then the negatively biased region became forward bias conditions for the diode.

After hydrogenation, electron emission was observed, starting at around −8 V in the forward-bias condition. The diode had a relatively high leakage current in the reverse bias region, while no emission current was detected. Before hydrogenation, no electron emissions were observed, even though the I_d–V curve was almost the same as that shown in Fig. 4.

In the forward bias region, I_d continuously increased up to −26 V, where I_e and η also exhibited a continuous rise, as shown in Fig. 4.

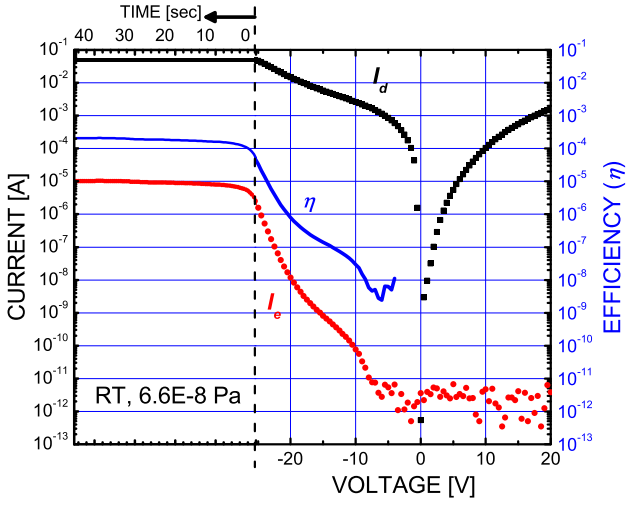

Fig. 4. The dependence of diode (I_d: filled squares) and emission currents (I_e: filled circles) on the applied voltage for the diode. Electron emission efficiency (η) is represented by the solid line. The electrode for the p-type layer was grounded, as shown in Fig. 1(b), and then the negatively biased region became forward bias conditions for the diode.

Above −26 V, a net current of 50 mA was obtained from this structure, where the current limit was set to control I_d.

Fig. 4 also showed the time dependence of I_d, I_e, and η after reaching the current limit. After several tens of seconds, I_e became 10 μA with an η of 0.02%, where the applied voltage decreased slightly (not shown).

3.2. p–i–n^+ junction diode

The detailed experimental procedure and the results from p–i–n^+ junction diodes such as those presented in Section 3.1 have already been reported in [27]. The thicknesses of the p-, i-, and n^+-layers were 200 nm, 130 nm, and 2 μm, respectively, while the distance between the electrode of the n^+-layer and the bottom of the mesa was 20 μm, which became the main component of the series resistance.

Fig. 5 shows the results of the I_d (filled squares) and I_e (filled circles) dependencies on the diode voltage. η is represented by a solid line. The electrode for the p-type layer was also grounded, as shown in Fig. 1(a), and the negatively biased region was in the forward bias condition. Above −81 V, the net current obtained was 5 mA, and the current limit was set to control I_d.

After hydrogenation, electron emissions were observed beginning at around −4 V under forward-bias conditions. For this diode, which is different from the n–i–p–p^+ diode, we used the n^+-layer that remarkably reduced the contact resistance [18]. Therefore, the threshold voltage that was observed for the emission was almost the same as the expected built-in potential. Before hydrogenation, no electron emissions were observed, even though the I_d–V curve was almost the same as that after hydrogenation. Leakage currents were detected in the reverse-bias region, but the diode showed no electron emission.

Fig. 5 also shows the time dependence of I_d, I_e, and η after reaching the current limit of 5 mA at −81 V in the forward-bias condition. After a few seconds, I_e became 8.8 μA with a η of 0.18%, as shown in Fig. 5.

4. Discussion

Electron emission currents were successfully obtained from both junction diodes during RT operation under forward bias conditions only after hydrogenation. These phenomena indicate that the electron

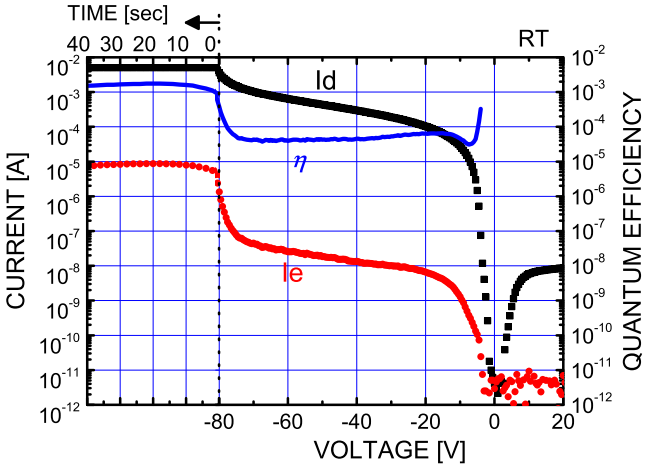

Fig. 5. The diode (I_d: filled squares) and emission currents (I_e: filled circles) dependences of a p–i–n^+ junction diode on diode voltage. Electron emission efficiency (η) is represented by the solid line. The electrode for p-type layer was grounded, and then negatively biased region became forward bias conditions for the diode.

emissions from these diodes are related to the NEA of the diamond surface.

In our experiments, we applied a current of 50 mA at −26 V to an n–i–p–p^+ diode, resulting in power consumption of 1.3 W, and 5 mA at 81 V to the p–i–n^+ diode, resulting in that of 0.4 W in the high current injection region. Under poor heat sinking conditions in vacuum, we should consider the possibility of thermionic emissions. We have not yet successfully measured the device temperature, but the temperature must increase above RT.

Some studies have reported thermionic emissions from nitrogen (N-) or phosphorous (P-) doped films [7,29–31]. For the N-doped case, a high thermionic emission performance was reported for heavily doped concentrations [N]$>10^{20}$ cm^{-3}, which is different from our diode cases. For the P-doped case, a current density of about 200 μA/cm^2 was reported for temperatures above 950 K. When we use an area of 3×10^{-4} cm^2 as the n top layer of our n–i–p–p^+ diode, it produces an emission current value of 0.06 μA, which is much smaller than the 10 μA in our case. While we still need to verify the degree of thermionic emission contribution, it appears to be very small in our case.

In addition, when we assume a significant rise in diode temperatures to explain the high current operation at RT, the η must decrease as the life times of free electrons and/or excitons are expected to decrease because of their increased recombination rate and the subsequent decrease in density. However, we observed an increase of η with increasing diode current. Therefore, in this discussion, we may ignore the heat-related problem in the high current injection region.

The emissions began when the applied bias voltage produced flat-band conditions, where the capacitance-voltage characteristics indicated carrier-injections in the i-layer. In summary, because of the flat-band condition, a significant relationship between carrier diffusion and the initiation of electron emissions from the p–i–n junction diodes is commonly observed. We denote these conditions as low current injection regions.

Under these conditions, η of the p–i–n^+ junction diode was about 5×10^{-5}, while that of n–i–p–p^+ was about 10^{-8}. We suggest two possible reasons for this. First, the η of a structure with a p top layer is 5000 times greater than that of a structure with an n top layer in the low current injection region. The electron emisison mechanism in the low current injection region appears to be dependent on the diode structure, in particular, on the carrier conduction type of the top layer of the diodes [32]. The second reason is that the contact resistance of metal/n-layer is too high for the injection of electrons because we observed a higher built-in potential in Figs. 3 and 4. Further investigations are necessary to clarify the mechanism in the low current injection region.

For the high current injection region where the emission current level was at around 10 μA, and with a diode current of 5–50 mA, each diode showed a nonlinear increase in electron emission current. The heavy doping techniques allowed such high net current levels during RT operation.

In this high current injection region, the p–i–n^+ junction diode showed η of 0.18%, and the n–i–p–p^+ diode showed η of 0.02%. The difference between these values is less than one order of magnitude, which is much smaller than 5000 in the low current injection region, as described above. Note that the η, which corresponds to the electron emission mechanism, depends on the diode current level, rather than the conduction type of the top layer.

According to the recent results of diamond DUV-LEDs mentioned in the introduction, the intensity of free exciton luminescence also exhibits a nonlinear increase for diode currents in similar current levels to the high current injection region described above. [17] Makino et al. explained that free excitons contribute to the nonlinear processes with their unique recombination processes in diamond.

The results of I_e saturation for a long time-constant as shown in Figs. 4 and 5 are interesting. During the period before settling occurs, carrier redistribution appears to occur near the p–i–n junction region under constant current operation, including electrons for emission current. In short, carrier redistribution depends on the conditions in diodes and the conditions of the electrons in vacuum. The time constant appears to be governed by heat as well as many other factors. Further experiments are needed in order to understand these phenomena.

Based on these interesting features, p–i–n junction diodes are promising as diamond cold cathodes with NEA during RT operation. We aim to continue our investigations in order to understand the emission mechanism in more detail.

5. Summary

Electron emission currents were successfully obtained for p–i–n junction diodes during room temperature (RT) operation under forward bias conditions only after hydrogenation.

The emissions began when the applied bias voltage produced flat-band conditions, where the C–V characteristics indicated carrier injection in the i-layer. In this low current injection region, the electron emission efficiency (η) for the p–i–n junction diodes (top is p-layer) was about 5×10^{-5}, while that for the n–i–p junction diodes (top is n-layer) was about 10^{-8}. With increasing diode current, both diodes showed an increase in η and a nonlinear increase in emission current. For a high diode current of 5–50 mA in high current injection region, both diodes generated emission currents of approximately 10 μA during RT operation, where η of the p–i–n junction diodes was 0.18%, while that of the n–i–p junction diodes was 0.02%.

Considering our previous results for diamond DUV-LEDs, we conclude that η, which corresponds to the electron emission mechanism, depended on the diode current level rather than the conduction type of the top layer in the high current injection region.

Acknowledgments

The authors would like to thank Prof. Dr. Ohashi, Dr. Nishizawa, Dr. Mizuochi and Dr. Miyazaki for their input in our group. This research was partially supported by the Industrial Technology Research Grant Program in 2008 from the New Energy and Industrial Technology Development Organization (NEDO) of Japan. A part of this work was conducted at the Nano-Processing Facility, supported by IBEC Innovation Platform, AIST.

References

[1] J.B. Cui, J. Ristein, L. Ley, Phys. Rev. B 59 (1999) 5847.
[2] J.L. Davidson, W.P. Kang, A. Wisitsora-At, Diamond Relat. Mater. 12 (2003) 429.
[3] D. Takeuchi, C.E. Nebel, S. Yamasaki, Phys. Stat. Sol. A 203 (2006) 3100.
[4] M.W. Geis, N.N. Efremow, J.D. Woodhouse, M.D. McAleese, M. Marchywka, D.G. Socker, J.F. Hochedez, Electr. Dev. Lett. 12 (1991) 456.
[5] G.R. Brandes, C.P. Beetz, C.A. Feger, R.L. Wright, Diamond Relat. Mater. 4 (1995) 586.
[6] T. Ito, M. Nishimura, A. Hatta, Appl. Phys. Lett. 73 (1998) 3739.
[7] K. Okano, T. Yamada, A. Sawabe, S. Koizumi, J. Itoh, G.A.J. Amaratunga, Appl. Phys. Lett. 79 (2001) 275.
[8] S. Koizumi: Ext. Abstr. (56th Spring Meet., 2009); Japan Society of Applied Physics and Related Societies, 1p-TC-11 [in Japanese].
[9] S. Kono, S. Koizumi, Surf. Sci. Nanotech. 7 (2009) 660 e-J.
[10] D. Takeuchi, H. Kato, G.S. Ri, T. Yamada, P.R. Vinod, D. Hwang, C.E. Nebel, H. Okushi, S. Yamasaki, Appl. Phys. Lett. 86 (2005) 152103.
[11] D. Takeuchi, T. Makino, H. Kato, I. Hirabayashi, H. Okushi, S. Yamasaki, Phys. Stat. Sol. A 9 (2010) 2093.
[12] S. Koizumi, M. Kamo, Y. Sato, H. Ozaki, T. Inuzuka, Appl. Phys. Lett. 71 (1997) 1065.
[13] H. Kato, T. Makino, S. Yamasaki, H. Okushi, J. Phys. D 40 (2007) 6189.
[14] D. Takeuchi, C.E. Nebel, S. Yamasaki, J. Appl. Phys. 99 (2006) 086102.
[15] C. Bandis, B.B. Pate, Phys. Rev. B 52 (1995) 12056.
[16] T. Makino, K. Yoshino, N. Sakai, K. Uchida, S. Koizumi, H. Kato, D. Takeuchi, M. Ogura, T. Matsumoto, H. Okushi, S. Yamasaki, in Abstract of Diamond 2010: 21st European Conference on Diamond, Diamond-Like Materials, Carbon Nanotubes, and Nitrides, 2010, p. O68, Budapest in Hungary.
[17] T. Makino, N. Tokuda, H. Kato, S. Kanno, S. Yamasaki, H. Okushi, Phys. Stat. Sol. A 205 (2008) 2200.
[18] H. Kato, H. Umezawa, N. Tokuda, D. Takeuchi, H. Okushi, S. Yamasaki, Appl. Phys. Lett. 93 (2008) 202103.

[19] N. Tokuda, H. Umezawa, T. Saito, K. Yamabe, H. Okushi, S. Yamasaki, Diamond Relat. Mater. 16 (2007) 767.
[20] T.H. Borst, O. Weis, Phys. Stat. Sol. A 154 (1996) 423.
[21] D. Takeuchi, M. Ogura, N. Tokuda, H. Okushi, S. Yamasaki, Phys. Stat. Sol. A 206 (2009) 1991.
[22] H. Oyama, S.-G. Ri, H. Kato, M. Ogura, T. Makino, D. Takeuchi, N. Tokuda, H. Okushi, S. Yamasaki, Appl. Phys. Lett. 94 (2009) 152109.
[23] T. Makino, H. Kato, S.-G. Ri, S. Yamasaki, H. Okushi, Diamond Relat. Mater. 17 (2008) 782.
[24] M. Suzuki, S. Koizumi, Phys. Stat. Sol. A 203 (2006) 3358.
[25] D. Takeuchi, M. Riedel, J. Ristein, L. Ley, Phys. Rev. B 68 (2003) 041304 R.
[26] M. Riedel, J. Ristein, L. Ley, Phys. Rev. B 69 (2004) 125338.
[27] D. Takeuchi, T. Makino, H. Kato, M. Ogura, N. Tokuda, K. Oyama, T. Matsumoto, I. Hirabayashi, H. Okushi, S. Yamasaki, Appl. Phys. Express 3 (2010) 041301.
[28] T. Makino, N. Tokuda, H. Kato, M. Ogura, H. Watanabe, S.-G. Ri, S. Yamasaki, H. Okushi, Jpn. J. Appl. Phys. 45 (2006) L1042.
[29] M. Suzuki, T. Ono, N. Sakuma, T. Sakai, Diamond Relat. Mater. 18 (2009) 1274.
[30] K. Kuriyama, C. Kimura, S. Koizumi, M. Kamo, T. Sugino, J. Vac. Sci. Technol. B 17 (1999) 723.
[31] F.A.M. Koeck, R.J. Nemanich, A. Lazea, K. Haenen, Diamond Relat. Mater. 18 (2009) 789.
[32] D. Takeuchi, T. Makino, S.-G. Ri, N. Tokuda, H. Kato, M. Ogura, H. Okushi, S. Yamasaki, Appl. Phys. Express 1 (2008) 015004.